applied sciences

MDPI

Article

Zinc Oxide-Based Rotational–Linear Triboelectric Nanogenerator

Achilleas Bardakas *, Apostolos Segkos and Christos Tsamis *

Institute of Nanoscience and Nanotechnology (INN), National Centre for Scientific Research "Demokritos", Patr. Gregoriou E & 27 Neapoleos Str., Aghia Paraskevi, 15310 Athens, Greece; a.segkos@inn.demokritos.gr
* Correspondence: a.bardakas@inn.demokritos.gr (A.B.); c.tsamis@inn.demokritos.gr (C.T.)

Abstract: In this study, we evaluate a prototype harvesting device that converts rotational motion to linear motion for harvesting rotational energy. Triboelectric materials are attached to the parts of the device that execute linear motion, resulting in a contact-separation mode of operation of triboelectric generators. As a triboelectric material, thin layers of ZnO nanoparticles deposited on Kapton films are evaluated. The design of the rotational–linear triboelectric nanogenerator (RL-TENG) exhibits several advantages since it does not suffer from the issues related to rotational tribogenerators such as wear and increased temperature during operation. Moreover, our approach can result in the modular design of energy-harvesting devices for a variety of applications. As a demonstrator, cups were attached to the rotating axis of the RL-TENG to harvest wind energy that is suitable for maritime applications.

Keywords: triboelectric nanogenerators; rotational energy; triboelectrification; TENGs; wind harvesting

Citation: Bardakas, A.; Segkos, A.; Tsamis, C. Zinc Oxide-Based Rotational–Linear Triboelectric Nanogenerator. *Appl. Sci.* **2024**, *14*, 2396. https://doi.org/10.3390/app14062396

Academic Editor: Huey Hoon Hng

Received: 12 February 2024
Revised: 7 March 2024
Accepted: 11 March 2024
Published: 12 March 2024

1. Introduction

Triboelectric harvesting has been identified as a very promising technology for the conversion of mechanical energy to electrical energy due to its low cost, abundance of available materials and high conversion efficiency even at low operating frequencies [1–5]. The operation of triboelectric generators (TENGs) is based on the charge exchange between two surfaces that are in contact (triboelectrification) and the subsequent electrostatic induction when these surfaces are set in relative motion. A major category of TENGs focuses on the conversion of rotational energy that could be induced by air and water flow, car wheels, etc. In general, rotating TENGs can be classified, according to their design, into two categories: (a) disk type and (b) cylindrical type. Further classification can be performed based on triboelectric materials (dielectric–dielectric or dielectric–conductor) and the operation mode (sliding, contact separation, non-contact). One of the first approaches of a segmented disk TENG was presented by Lin et al. [6]. The tribogenerator was based on sliding triboelectrification and periodic overlapping of the segmented disks due to rotation. Large output currents were obtained at a high frequency (117.6 μA and 29.0 mA/cm^2 of 66.7 Hz at a rotating speed of 1000 rpm). An updated version of the disk generator was later presented by the same group [7] in order to improve the operational characteristics, the longevity and the stability of the device. The new design was based on a freestanding triboelectric layer on the rotational disk, while the electrodes were located onto the stationary disk. Zhang et al. [8] presented a direct-current triboelectric nanogenerator (DC-TENG) based on a rotating-disk design. It consisted of two disks and two pairs of carbon fiber flexible brushes that contacted the electrodes. Due to its design, the tribogenerator was serving as a constant current source for direct driving electronic devices.

Bai et al. [9] demonstrated a cylindrical rotating triboelectric nanogenerator (TENG) based on sliding electrification. The TENG was based on a core–shell structure with an alternative strip on the surface. During rotation, the relative sliding between the contact surfaces of the core and the shell results in an "in-plane" lateral polarization that drives the external current. A power density of 36.9 W/m^2 was obtained by a rotating TENG

with 8 strip units at a rotation rate of 1000 rpm. Zhang et al. [10] presented a non-contact cylindrical rotating TENG for harvesting mechanical energy from water flow such as that in pipes and sewers. The generator was operated in freestanding mode between two rotating interfaces to minimize abrasion of the electrodes. When placed in water flow, the output voltage and the current of the TENG reached 1670 V and 13.4 μA, respectively. An eccentric-type TENG, consisting of a fixed metal electrode, a rotor-independent layer and a base, was proposed by Qu et al. [11]. Due to its design, the TENG could effectively reduce the wear of the friction layer and improve the durability of devices. A rolling friction contact-separation mode triboelectric generator was presented by Yang et al. [12] that was fabricated for harvesting vertical rotation energy by utilizing the integrated cylindrical surface with the conjunction of rolling contact electrification and electrostatic induction. Several rotational TENGs have also been presented for harvesting wind energy [13]. For instance, Park et al. [14] developed a continuously rotating TEG, aiming to operate at marginal wind velocities by maximizing the efficiency of the sliding contact, which was a one-dimensional fiber rather than a 2D contact area. A ring-type TENG for rotational energy harvesting was presented by Xin et al. [15]. The device could also be used as a self-powered rotational speed sensor. These are only some examples of the various designs that have been presented for harvesting rotational energy. A detailed presentation of rotational triboelectric generators can be found in [16].

An alternative design for the conversion of rotational energy was demonstrated by Mo et al. [17]. They developed a self-powered air filter for the removal of particulate matter from the environment based on a radial piston TENG. In this study, we propose a novel design for harvesting rotational energy that is based on the transformation of rotational motion to linear motion, allowing for TENGs to operate at contact-separation mode and thus minimizing the inherent issues of rotating TENGs, such as wear and the development of high temperatures.

2. Materials and Methods

2.1. Design and Fabrication of the Rotational–Linear Tribogenerators (RL-TENG)

For the design of the RL-TENG, Autodesk Fusion360 was used, while the fabrication of the device was performed using a 3D printer (Creality Ender 7). The main printing parameters are as follows:

1. Material: PETG (polyethylene terephthalate glycol);
2. Layer height: 0.2 mm;
3. Perimeters: 4;
4. Infill: 40% (triangles).

The design of the RL-TENG is shown in Figure 1a. It consists of (a) 3 pairs of contact-separation type triboelectric generators, i.e., T1, T2, T3 (Figure 1b), (b) the circular base upon which the TENGs are mounted and (c) a circular cam that is attached to the axis of rotation and is perpendicular to the base plane.

In Figure 1c, we can see a part of a triboelectric pair. The triboelectric material was placed on the surface of the component using double-sided aluminum tape. The area of the triboelectric surfaces that contacted each other is 1×1.67 cm^2. Figure 2 is a photograph of the RL-TENG. We can identify the three triboelectric pairs, i.e., T1, T2 and T3, as well as their wiring. In the central area of the tribogenerator, the cam is placed (not shown in the figure). Two different cams were used to control whether the triboelectric pairs worked in a synchronous or asynchronous way. The cam is mounted to the rotating axis (vertical to the plane, not shown in figure) to provide the rotational motion.

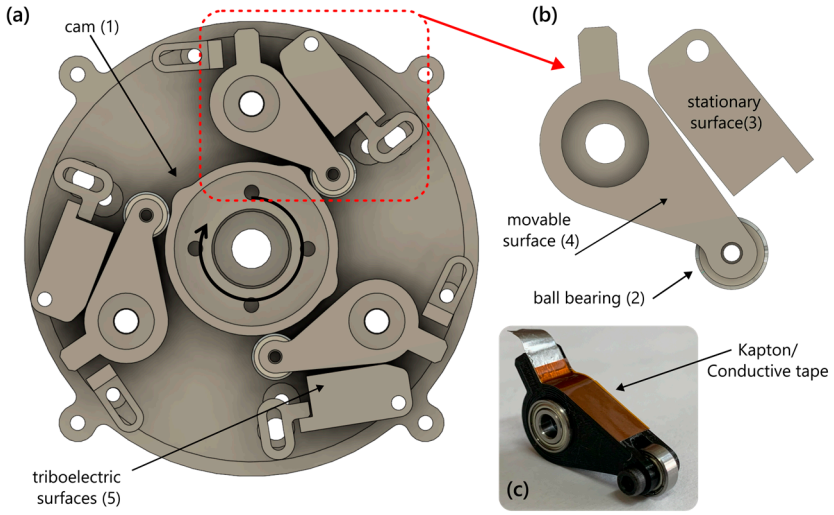

Figure 1. (**a**) Schematic of the energy-harvesting device, (**b**) a magnified view of a triboelectric pair showing the movable and stationary triboelectric surfaces and (**c**) a part of a triboelectric pair.

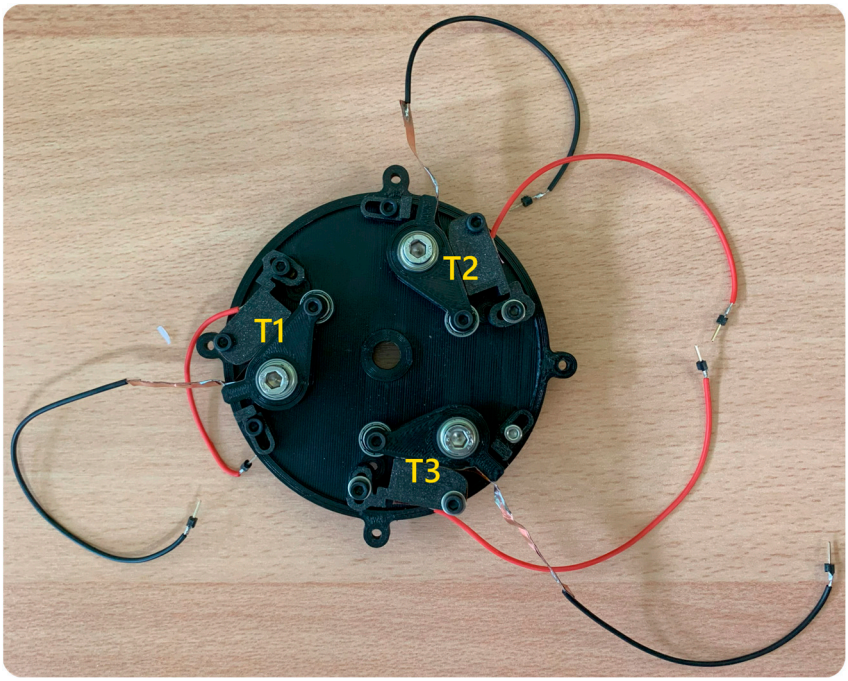

Figure 2. Photograph of the RL-TENG. We can identify the three triboelectric pairs (T1, T2 and T3).

For the triboelectric layers, Kapton® (DuPont™, Kingston, ON, Canada) and Kapton® with a ZnO thin film deposited by sol–gel on the surface were used. The thickness of both Kapton® layers was 75 µm. Briefly, a sol–gel solution was prepared by dissolving the appropriate amount of Zinc Acetate Dihydrate ($C_4H_{10}O_6Zn$, Merck, Germany, and urea ($CO(NH_2)_2$, The Science Company, Lakewood, CO, USA) in ethanol (C_2H_5OH, Carlo Erba Reagents, Emmendingen, Germany) using magnetic stirring, at 60 °C for 30 min, in order to end up with a 40 mM solution containing 5w/w% of urea. The sol–gel was left to cool to room temperature prior to use for 24 h. ZnO films were prepared by ten successive spin coatings on Kapton films. After each deposition, the film was annealed at 300 °C in air. A detailed description of the ZnO thin-film fabrication and deposition process as well as its performance as a triboelectric layer can be found in [18].

2.2. Characterization Setup

For the characterization of the RL-TENG, the setup shown in Figure 3a was used. It consists of an aluminum base with threaded holes for ease of mounting the required components. A DC servo motor (PD4-CB59M024035-E-01) attached to an aluminum profile extrusion was used to provide rotational motion, powered by a 24 V power supply (350 W) and controlled via USB. The Plug&Drive Studio 2 computer UI (Nanotec Electronic GmbH & Co. KG, Feldkirchen, Germany) was utilized for tuning and controlling the rotational speed of the servo motor. The RL-TENG was mounted on the rotational axis of the servo motor using a 3D-printed mounting plate with the appropriate spacers, as shown in Figure 3b.

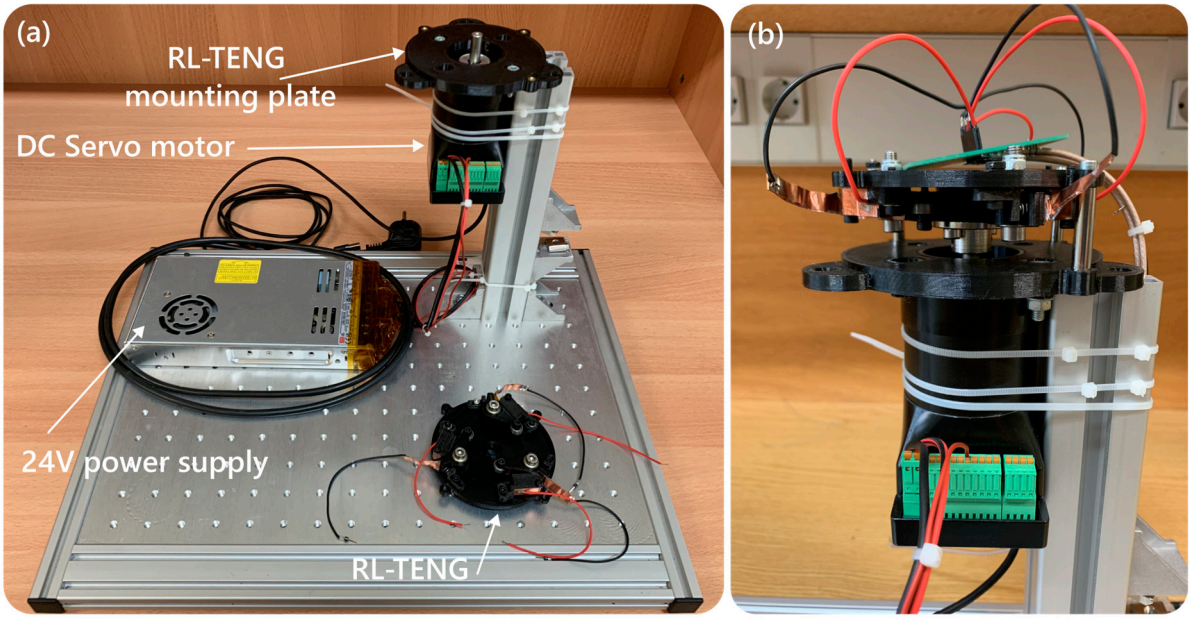

Figure 3. (**a**) The experimental setup used in the electrical characterization of the RL-TENG; (**b**) the RL-TENG mounted on top of the servo motor, aligned with the axis of rotation.

2.3. Electrical Measurements

Four types of measurements were performed: (a) time-dependent output voltage (transient), (b) capacitor charging, (c) open circuit voltage (V_{oc}) and (d) short circuit current (Isc). For the transient measurements, the RL-TENG was connected to an InfiniiVision DSO7104A oscilloscope (Agilent Technologies, Santa Clara, CA, USA) through a 10× probe, terminated at 1 MΩ input impedance. For the capacitor charging measurements, a full, quad bridge rectifier circuit was used. The capacitor voltage was monitored by a Keithley 617 electrometer (Keithley, Solon, OH, USA), with an input resistance of 200 TΩ. For the measurement of the short circuit current Isc, a Stanford Research Systems SR570 (Stanford Research Systems, Sunnyvale, CA, USA) low-noise current preamplifier was used. For the estimation of the power as a function of an external load, the methodology developed by Jayasvasti et al. [19] was adapted. In brief, the methodology consists of adding a small resistance (1 MΩ) in parallel with the oscilloscope probe (input resistance: 10 MΩ) to reduce the current flowing through the measuring device. It was demonstrated that this methodology is more accurate for the extraction of the power output compared to the typical method of measuring the voltage drop across the load. From the same measurements, the open circuit voltage can be estimated. All experiments were performed at 25 ± 2 °C and 25 ± 3%RH (relative humidity).

3. Results and Discussion

3.1. Operating Principle of Tribogenerators in Contact-Separation Mode

As we have described above, the RL-TENG is based on the transformation of rotational motion to linear motion. The output voltage of RL-TENG is a combination of the output voltages of each triboelectric pair T1, T2 and T3 that operate in contact-separation mode. In this operation mode, the movable part (active TENG in Figure 4a) is moving in a vertical direction relative to the stationary part (base TENG in Figure 4a). When the two triboelectric surfaces (Kapton and ZnO-on-Kapton) are in contact, charges with different polarities appear on the two materials, due to contact electrification. The type of charge that appears on each material depends on the electronegativity of the two materials. In our case, the surface of ZnO is charged positively, and the surface of Kapton is charged negatively, due to the differences in the electronegativities of the two materials. As the two triboelectric surfaces start moving away from each other, a charge build up will appear at the electrodes, located at the backside of the triboelectric materials, and a current will flow in the external circuit. A detailed theoretical analysis of the triboelectric nanogenerators in contact-separation mode has been presented by Niu et al. [20] al and Dharmasena et al. [21].

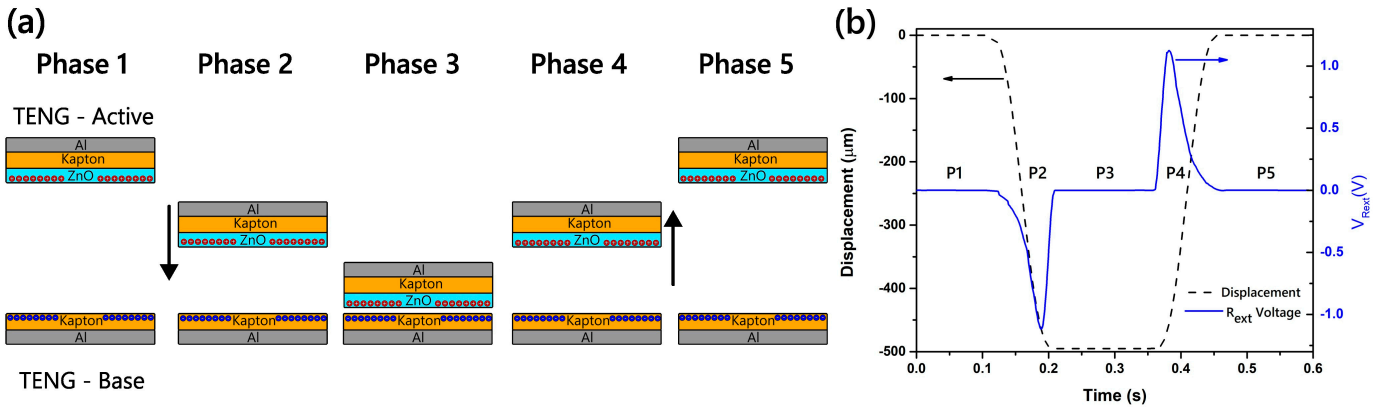

Figure 4. (**a**) Different phases of a triboelectric generator in contact-separation mode; (**b**) simulation results of the modeled tribogenerator, showing the output voltage during each phase.

Figure 4a illustrates schematically the TENG operation in contact-separation mode. Assuming that there are already charges developed on the active and the base surfaces of the tribogenerator, we can distinguish five different phases during an operation cycle.

- Phase 1: The active area is stationary at its balance position. No current flows through the external circuit.
- Phase 2: The active area begins moving until it reaches the position of maximum displacement. Current flows to the external circuit due to electrostatic induction. The current flow takes place for the duration of the movement of the active area.
- Phase 3: The active area remains still at the maximum displacement for a short amount of time. No current flows through the external circuit.
- Phase 4: The active area starts moving backwards towards its balance position. Current flows to the external circuit due to electrostatic induction, but in the opposite direction relative to phase P2.
- Phase 5: The active area reaches its maximum position and stops moving. No current flows through the external circuit.

During all the phases described above, the reference surface (TENG-Base) remains in the same position.

To analyze the electrical performance of the tribogenerator during these phases, we have modeled and simulated the device in COMSOL 5.0. For the simulation, the following parameters were used: thickness of Kapton: 50 μm; relative permittivity of Kapton: 3; and surface charge density: 50 $\mu C/m^2$. ZnO layer was omitted in the simulation since

it is several orders of magnitude smaller compared to Kapton. Figure 4b shows the output voltage of the tribogenerator, connected to an external load resistance R_{ext} (=1 MΩ), during the various phases. As expected, voltage develops between the electrodes, due to electrostatic induction, when the two electrodes are in relative motion.

3.2. Characterization of the RL-TENG

The triboelectric pairs were measured for various rotational velocities using the setup shown in Figure 1. Figure 5 shows the transient signal of triboelectric pair T1 as a function of time for rotational velocities ranging from 60 rpm to 300 rpm. We notice that, as the rotational velocity increases, the triboelectric signal increases. In fact, the output voltage signal increases from 0.2 V for 60 rpm to 2 V for 300 rpm.

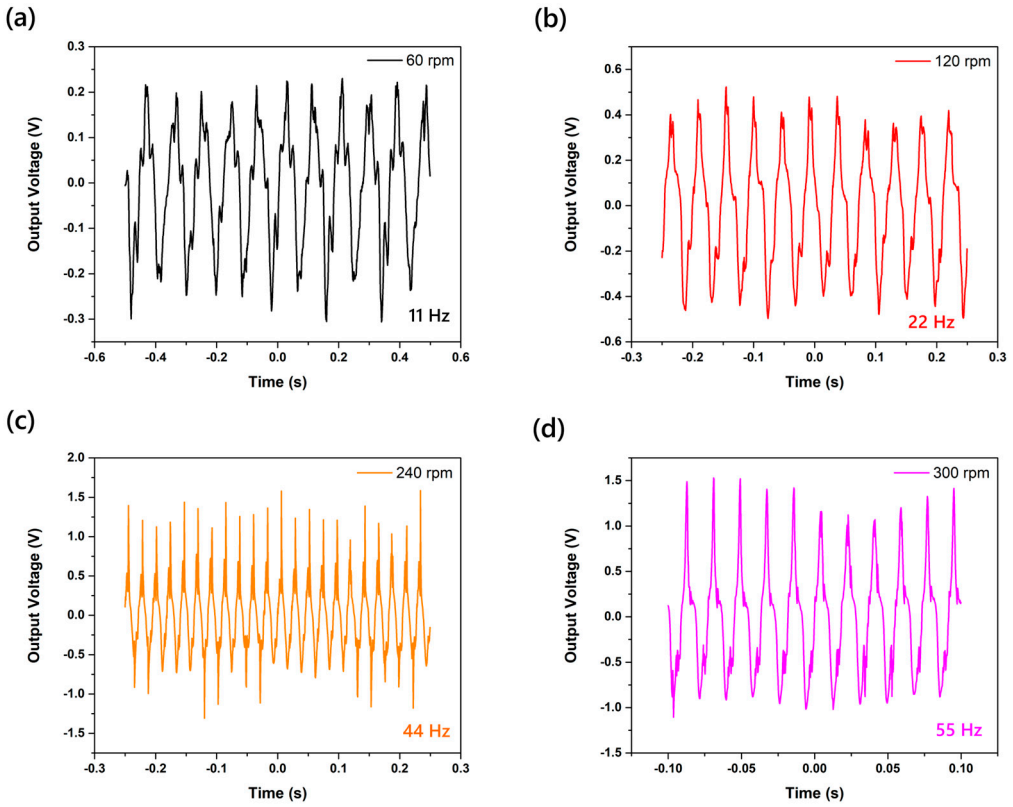

Figure 5. Output signal of T1 triboelectric pair of RL-TENG for various rotational velocities: (**a**) 60 rpm, (**b**) 120 rpm, (**c**) 240 rpm and (**d**) 300 rpm. (Output voltage frequency is a multiple of the number of cams located on each disk, in this case 11).

Figure 6a,b show the output current and voltage of triboelectric pair T1 as a function of the external load for various rotational velocities. The short circuit current increases from 133 nA to 267 nA, and the open circuit voltage increases from 2.24 V to 3 V as the rotational velocity of the RLTENG increases from 100 rpm to 300 rpm. Figure 6c shows the output power as a function of the rotational speed. The output power increases from 0.1 μW to 0.23 μW for the same rotational velocities. Maximum output power is obtained when the resistance value of the external load is 20 MΩ. Similar results are obtained from triboelectric pairs T2 and T3, although small differences are observed due to variations in the manufacturing and assembly process.

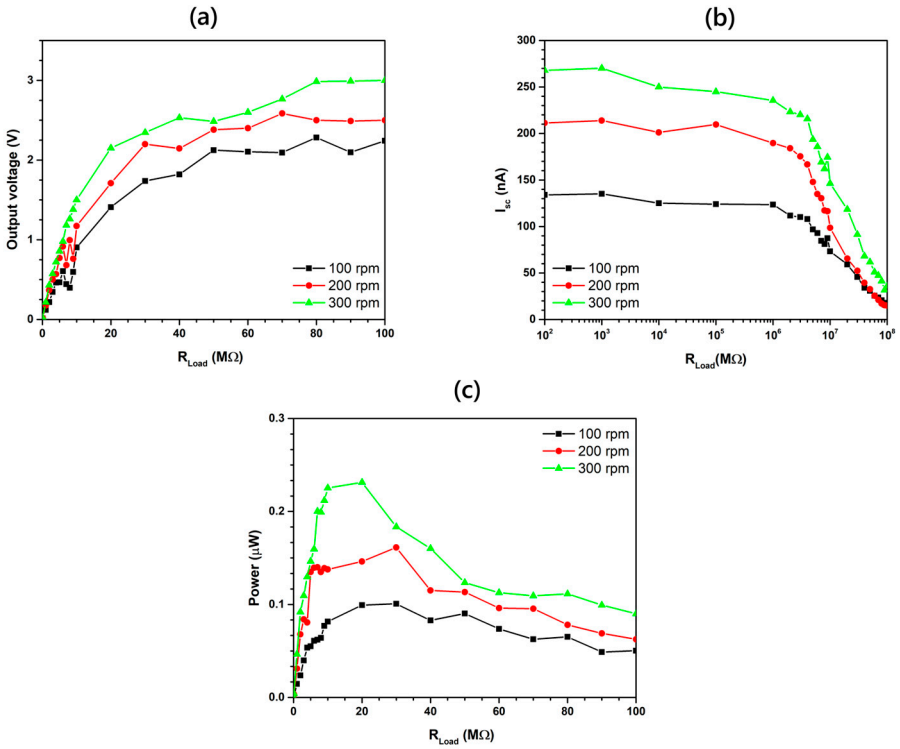

Figure 6. (**a**) Output voltage, (**b**) output current and (**c**) output power of the T1 triboelectric pair of the RL-TENG as a function of the external load for rotational velocities ranging from 100 to 300 rpm.

3.3. Connectivity of the Triboelectric Pairs

Since the RL-TENG consists of three triboelectric pairs, a question that has been raised is how to connect them in order to obtain the maximum power from the device. One obvious approach is to connect each triboelectric pair with a bridge rectifier and then connect the outputs together either in series or in parallel. Such a solution has been proven to be an efficient way for scavenging the total amount of generated energy [17]. However, this means that we need to use three separate bridge rectifiers, increasing the complexity of the electronic components required for device operation. To avoid that, we have implemented an alternative approach. We have investigated the influence of the total stored energy for two different cams: (a) During the rotation of the first cam (disk A, Figure 7a), the tribogenerators are moving in phase as can be seen from Figure 7b, where we notice that the triboelectric signal of T1 and T3 are almost identical. (b) During the rotation of the second cam (disk B, Figure 7c), the tribogenerators are out of phase, and only one triboelectric pair is set in motion during a specific time interval, as can be seen in Figure 7d, where we notice that T1 is active when T3 is inactive. As a metric for the comparison between the two methods, we use the energy stored in a capacitor using a single bridge rectifier during charging.

Figure 8 shows the energy stored at the capacitor as a function of time for triboelectric pairs T1 and T3 for two rotational velocities, i.e., 60 rpm (Figure 8a) and 300 rpm T3 (Figure 8b), when disk B is used. In the same figures, we see the energy stored when the triboelectric pairs are connected in parallel prior to the rectifier. We see that the energy of the combined triboelectric pairs is higher compared to each individual pair. Assuming that the total energy that should be stored in the capacitor is the sum of the energies that are stored in each triboelectric pair, from the analysis of the data, we see that for low rotational velocities, the stored energy is 67% of the total energy. However, as the rotational velocity increases, the amount of stored energy is reduced reaching 56% at 300 rpm. This energy loss is probably due to the random signal generated from the triboelectric pairs due to vibrations caused during device operation. These signals interfere in a destructive way,

cancelling out each other and reducing the amount of stored energy. Similar results were obtained when disk A was used.

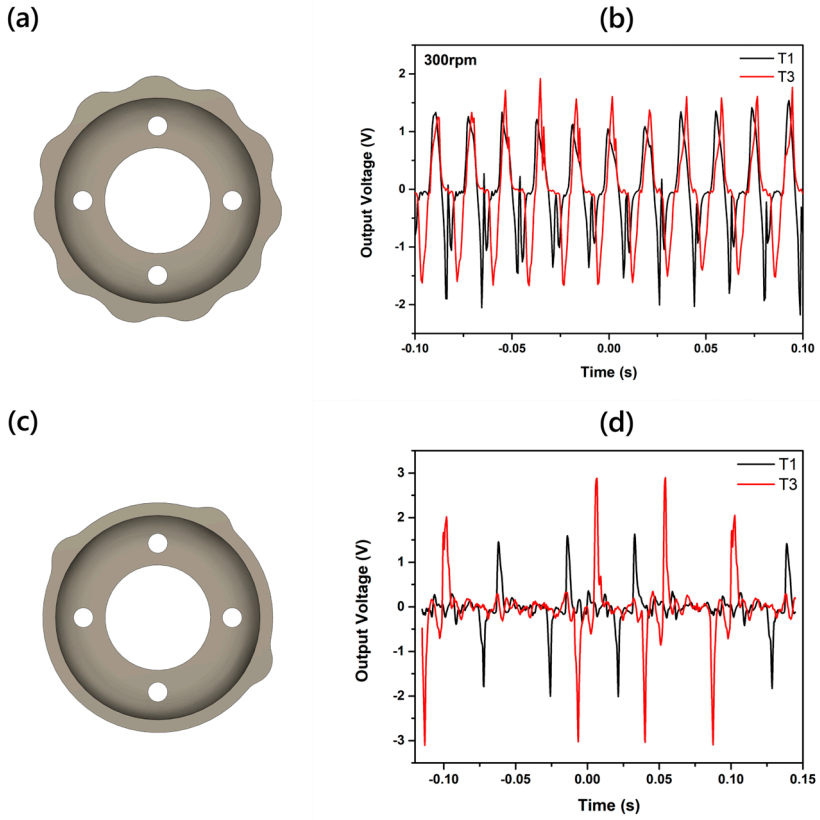

Figure 7. (**a**) Disk A for in-phase operation of triboelectric pairs, (**b**) output voltage of T1 and T3 for disk A, (**c**) disk B for out-of-phase operation of triboelectric pairs and (**d**) output voltage of T1 and T3 for disk B.

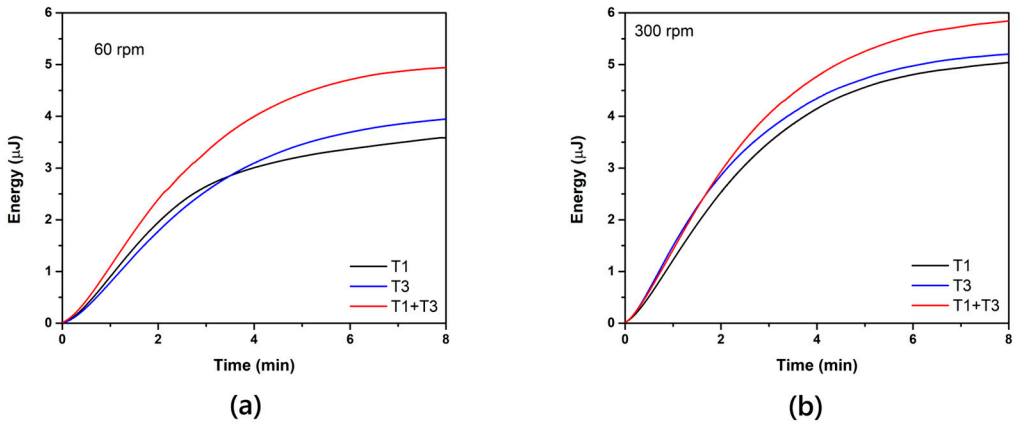

Figure 8. Energy stored in the capacitor as a function of time after charging for rotational velocities (**a**) 60 rpm and (**b**) 300 rpm.

3.4. Optimization of Performance Characteristics

From the analysis of the results, we see that the electrical performance of the RL-TENG is inferior to what we would anticipate compared to the results that we obtained for the Kapton/ZnO layers in previous experiments. When the same triboelectric surfaces of area 2×2 cm^2 were evaluated [18], the output voltage reached about 20 V, the short circuit current 12 μA, the open circuit voltage 105 V and the maximum output power 350 μW, which is much higher compared to the results obtained for a single triboelectric pair. To

some extent, this is expected since the surface area of the triboelectric areas T1, T2 and T3 is reduced compared to the previous ones by 2.4 times (1.67 cm^2 compared to 4 cm^2).

There are also other parameters that could influence the triboelectric performance that are related to the operational principle of the triboelectric generator. Being a transient phenomenon, the triboelectric signal will depend strongly on the relative velocity between the two surfaces. Taghavi et al. [22] showed that the relative velocity of the triboelectric surfaces affects the instantaneous signal as well as the average power of TENGs. They also provided evidence that the separation phase of the two triboelectric surfaces could also impact the electrical performance of the tribogenerator. Another parameter that affects the triboelectric signal is the contact force that develops between the two triboelectric surfaces. Vasandani et al. [23] studied theoretically and experimentally the influence of the contact force of the triboelectric signal TENG using a PDMS film with microdome patterns. As a reference electrode, a PET film was used. The triboelectric signal was measured against a PET reference surface. They demonstrated that, by changing the contact force from 4.4 N to 5.1 N, the triboelectric signal increased by 100%.

To verify the influence of the above-mentioned parameters (surface area and transition time/force) on the triboelectric signal, we have fabricated a part of a more robust prototype tribogenerator. In this case, the surface area of the prototype was the same as that of the test triboelectric generators (Figure 9a). In addition, we have enhanced the mechanical stability of the structure and used a stronger return spring. Typical results are shown in Figure 9b. We see that the maximum voltage per tap is 12 V for a rotational velocity of 350 rpm. Moreover, the maximum power per tap is 10 times more compared to that of the triboelectric pairs used in the RL-TENG. Our results indicate that, with a more robust structure and with larger triboelectric contact areas, significantly enhanced performance can be obtained for the RL-TENG.

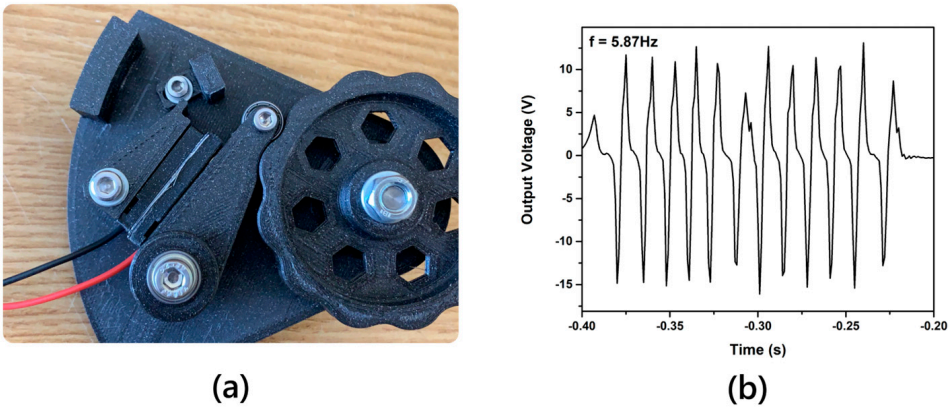

Figure 9. (**a**) Part of a more robust triboelectric generator and (**b**) output voltage as a function of time at 350 rpm.

3.5. Application for Harvesting Wind Energy

The RL-TENG was adapted to be a wind-harvesting device as shown in Figure 10a. The wind-harvesting device is composed of (a) a case that encloses the RL-TENG for mechanical support, providing a way for the vertical shaft to spin freely using deep-groove ball bearings, (b) the vertical shaft where the cam is mounted using an aluminum adapter and (c) three cups attached to the vertical shaft. As the wind blows, the cups create rotational torque, spinning the vertical shaft and as consequence the RL-TENG, as shown in Figure 10b (Video S1). For measuring the air velocity, a hand-held anemometer was utilized (UT363BT, UNI-T®, Dongguan, China) that provided real-time and data logging capabilities via Bluetooth®, displayed at a smartphone app (iENV2.0, UNI-T®).

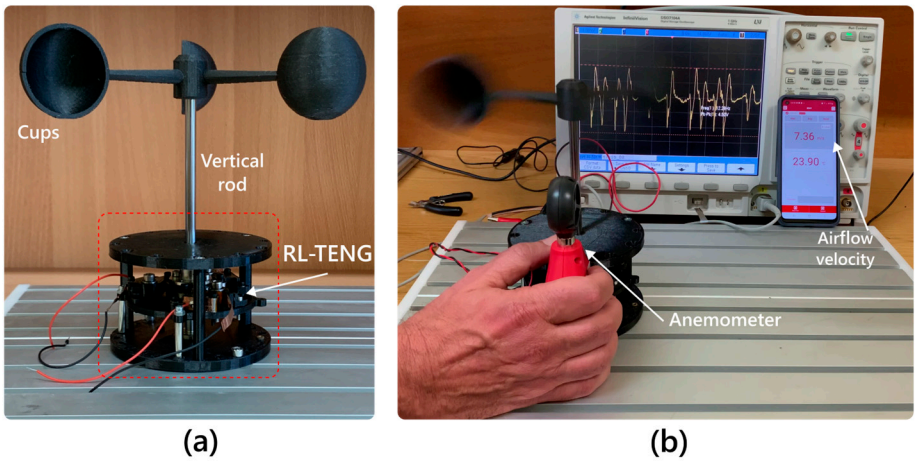

Figure 10. (**a**) RL-TENG attached to the wind-harvesting device and (**b**) setup for the wind-harvesting experiments.

Figure 11 shows the power generated by each triboelectric pair as a function of the wind velocity. We see that the different triboelectric pairs do not have the same performance. This is normal since the different pairs were prepared, to some extent, manually and not with a standardized manufacturing and assembly process. Moreover, the rotational speed of the device as a function of the wind velocity is presented in Figure 11b. We see that there is a very good match between the triboelectric pairs for which the measurements were not performed simultaneously.

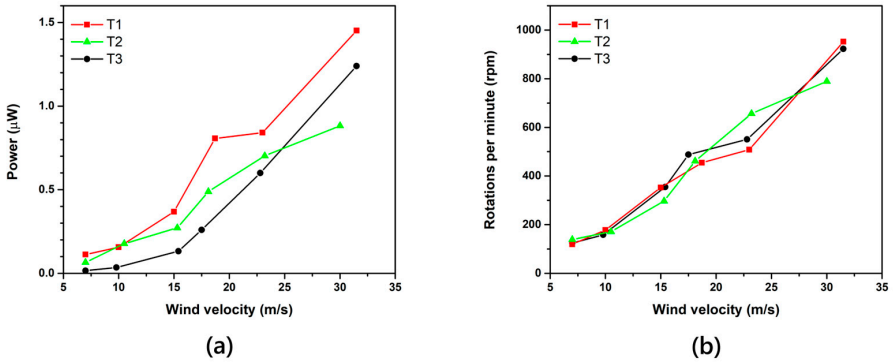

Figure 11. (**a**) Maximum power delivered by each triboelectric pair as a function of the wind velocity. (**b**) Rotational velocity of the RL-TENG as a function of wind velocity.

3.6. Advantages of the Proposed RL-TENG

Compared to the already available rotational tribogenerators, RL-TENG presents several advantages including the following:

1. Since RL-TENG operates in contact-separation mode, material wear is minimized compared to conventional rotational tribogenerators where continuous contact (in sliding mode) is required at high rotational velocities. It is thus expected that the operational time of the proposed RL-TENG will be significantly higher compared to that of rotational devices.
2. Since there is no sliding between the two triboelectric surfaces, no high temperatures are developed because of friction.
3. Due to its design, several material combinations can be easily used as triboelectric materials. By selecting a material combination that is further away in the triboelectric series, the triboelectric signal can be significantly increased.
4. It can be scaled up by increasing its size both radially as well as vertically to increase the surface area and thus improve the tribogenerator's performance. Another way to

increase the surface would be to implement origami-inspired structures which have been demonstrated to significantly increase triboelectric performance [24,25].

5. Another way to enhance the output performance of the RL-TENG is to use hybrid energy-harvesting approaches, such as combining piezoelectric, triboelectric and electromagnetic generators in a single device [25]. The advantage of the proposed design is that it can be easily adjusted to exploit all performance improvements that have been demonstrated for contact-separation mode tribogenerators [26].
6. It can be assembled in a modular way.
7. It can be fabricated using simple mechanical parts with reduced cost, increased lifetime and simple maintenance.

4. Conclusions

In this study, we have presented a rotational-based triboelectric generator based on a novel design. The proposed RL-TENG consists of three triboelectric pairs that operate in contact-separation mode, providing an alternative power generation mechanism in contrast to conventional rotational tribogenerators, mitigating the inherent problems found in common rotating tribogenerators such as the development of high temperature and increased material wear due to friction. The experimental results present the output characteristics of the RL-TENG, showing a clear dependence of open-circuit voltage, short-circuit current and output power for a wide range of rational speeds, with a maximum power of 0.23 μW at 20 MΩ and 300 rpm. The effect of connectivity between the triboelectric pairs was also explored showing that out-of-phase operation (disk B) does not require separate rectification for every triboelectric pair, reducing complexity and offering increased energy storage by connecting the pairs in parallel. Finally, a wind-harvesting device was developed, which presents the potential of the proposed RL-TENG in harvesting applications utilizing pure rotational motion and is able to provide power up to 1000 rpm. In conclusion, the proposed design provides flexibility, can be easily adapted to a variety of harvesting applications, exhibits ease of maintenance, has an ability to operate on a wide range of rotational velocities with reduced wear and can be optimized for the specific application by tailoring the relative contact velocity, contact force and contact surface between the triboelectric surfaces.

Supplementary Materials: The following supporting information can be downloaded at: https://www.mdpi.com/article/10.3390/app14062396/s1, Video S1: RL-TENG wind experiments.

Author Contributions: Conceptualization, A.B., A.S. and C.T.; methodology, A.B. and A.S.; validation, A.B. and C.T.; writing—original draft preparation, A.B.; writing—review and editing, all authors; supervision, C.T.; funding acquisition, C.T. All authors have read and agreed to the published version of the manuscript.

Funding: This research has been co-financed by the European Union and Greek national funds through the Operational Program Competitiveness, Entrepreneurship and Innovation, under the call RESEARCH-CREATE-INNOVATE (EFOS, project code: T2EΔK-00350).

Data Availability Statement: The raw data supporting the conclusions of this article will be made available by the corresponding authors on request.

Acknowledgments: The author acknowledge E. Hinari for the preparation of ZnO-based triboelectric surfaces.

Conflicts of Interest: The authors declare no conflicts of interest.

References

1. Choi, D.; Lee, Y.; Lin, Z.H.; Cho, S.; Kim, M.; Ao, C.K.; Soh, S.; Sohn, C.; Jeong, C.K.; Lee, J.; et al. Recent Advances in Triboelectric Nanogenerators: From Technological Progress to Commercial Applications. *ACS Nano* **2023**, *17*, 11087–11219. [CrossRef] [PubMed]
2. Yu, Y.; Li, H.; Zhao, D.; Gao, Q.; Li, X.; Wang, J.; Wang, Z.L.; Cheng, T. Material's Selection Rules for High Performance Triboelectric Nanogenerators. *Mater. Today* **2023**, *64*, 61–71. [CrossRef]

3. Delgado-Alvarado, E.; Elvira-Hernández, E.A.; Hernández-Hernández, J.; Huerta-Chua, J.; Vázquez-Leal, H.; Martínez-Castillo, J.; García-Ramírez, P.J.; Herrera-May, A.L. Recent Progress of Nanogenerators for Green Energy Harvesting: Performance, Applications, and Challenges. *Nanomaterials* **2022**, *12*, 2549. [CrossRef] [PubMed]
4. Zhang, R.; Örtegren, J.; Hummelgård, M.; Olsen, M.; Andersson, H.; Olin, H. A Review of the Advances in Composites/Nanocomposites for Triboelectric Nanogenerators. *Nanotechnology* **2022**, *33*, 212003. [CrossRef] [PubMed]
5. Chao, S.; Ouyang, H.; Jiang, D.; Fan, Y.; Li, Z. Triboelectric Nanogenerator Based on Degradable Materials. *EcoMat* **2021**, *3*, e12072. [CrossRef]
6. Lin, L.; Wang, S.; Xie, Y.; Jing, Q.; Niu, S.; Hu, Y.; Wang, Z.L. Segmentally Structured Disk Triboelectric Nanogenerator for Harvesting Rotational Mechanical Energy. *Nano Lett.* **2013**, *13*, 2916–2923. [CrossRef] [PubMed]
7. Lin, L.; Wang, S.; Niu, S.; Liu, C.; Xie, Y.; Wang, Z.L. Noncontact Free-Rotating Disk Triboelectric Nanogenerator as a Sustainable Energy Harvester and Self-Powered Mechanical Sensor. *ACS Appl. Mater. Interfaces* **2014**, *6*, 3031–3038. [CrossRef]
8. Zhang, C.; Zhou, T.; Tang, W.; Han, C.; Zhang, L.; Wang, Z.L. Rotating-Disk-Based Direct-Current Triboelectric Nanogenerator. *Adv. Energy Mater.* **2014**, *4*, 1301798. [CrossRef]
9. Bai, P.; Zhu, G.; Liu, Y.; Chen, J.; Jing, Q.; Yang, W.; Ma, J.; Zhang, G.; Wang, Z.L. Cylindrical Rotating Triboelectric Nanogenerator. *ACS Nano* **2013**, *7*, 6361–6366. [CrossRef]
10. Zhang, N.; Qin, C.; Feng, T.; Li, J.; Yang, Z.; Sun, X.; Liang, E.; Mao, Y.; Wang, X. Non-Contact Cylindrical Rotating Triboelectric Nanogenerator for Harvesting Kinetic Energy from Hydraulics. *Nano Res.* **2020**, *13*, 1903–1907. [CrossRef]
11. Qu, Z.; Huang, M.; Dai, R.; An, Y.; Chen, C.; Nie, G.; Wang, X.; Zhang, Y.; Yin, W. Using Non-Contact Eccentric Nanogenerator to Collect Energy Continuously under Periodic Vibration. *Nano Energy* **2021**, *87*, 106159. [CrossRef]
12. Yang, H.; Liu, W.; Xi, Y.; Lai, M.; Guo, H.; Liu, G.; Wang, M.; Li, T.; Ji, X.; Li, X. Rolling Friction Contact-Separation Mode Hybrid Triboelectric Nanogenerator for Mechanical Energy Harvesting and Self-Powered Multifunctional Sensors. *Nano Energy* **2018**, *47*, 539–546. [CrossRef]
13. Dong, X.; Liu, Z.; Yang, P.; Chen, X. Harvesting Wind Energy Based on Triboelectric Nanogenerators. *Nanoenergy Adv.* **2022**, *2*, 245–270. [CrossRef]
14. Park, S.; Ryu, H.; Park, S.; Hong, H.; Jung, H.Y.; Park, J.J. Rotating Triboelectric Generator Using Sliding Contact and Noncontact from 1D Fiber Friction. *Nano Energy* **2017**, *33*, 184–194. [CrossRef]
15. Xin, Y.; Du, T.; Liu, C.; Hu, Z.; Sun, P.; Xu, M. A Ring-Type Triboelectric Nanogenerator for Rotational Mechanical Energy Harvesting and Self-Powered Rotational Speed Sensing. *Micromachines* **2022**, *13*, 556. [CrossRef] [PubMed]
16. Segkos, A.; Tsamis, C. Rotating Triboelectric Nanogenerators for Energy Harvesting and Their Applications. *Nanoenergy Adv.* **2023**, *3*, 170–219. [CrossRef]
17. Mo, J.; Zhang, C.; Lu, Y.; Liu, Y.; Zhang, N.; Wang, S.; Nie, S. Radial Piston Triboelectric Nanogenerator-Enhanced Cellulose Fiber Air Filter for Self-Powered Particulate Matter Removal. *Nano Energy* **2020**, *78*, 105357. [CrossRef]
18. Hinari, E.; Bardakas, A.; Tsamis, C. Enhancement of the performance of ZnO-based triboelectric generators by nitrogen doping. *Energy Harvest. Syst.* **2024**. *submitted*.
19. Jayasvasti, S.; Thainiramit, P.; Yingyong, P.; Isarakorn, D. Technique for Measuring Power across High Resistive Load of Triboelectric Energy Harvester. *Micromachines* **2021**, *12*, 766. [CrossRef]
20. Niu, S.; Wang, S.; Lin, L.; Liu, Y.; Zhou, Y.S.; Hu, Y.; Wang, Z.L. Theoretical Study of Contact-Mode Triboelectric Nanogenerators as an Effective Power Source. *Energy Environ. Sci.* **2013**, *6*, 3576–3583. [CrossRef]
21. Dharmasena, R.D.I.G.; Jayawardena, K.D.G.I.; Mills, C.A.; Dorey, R.A.; Silva, S.R.P. A Unified Theoretical Model for Triboelectric Nanogenerators. *Nano Energy* **2018**, *48*, 391–400. [CrossRef]
22. Taghavi, M.; Beccai, L. A Contact-Key Triboelectric Nanogenerator: Theoretical and Experimental Study on Motion Speed Influence. *Nano Energy* **2015**, *18*, 283–292. [CrossRef]
23. Vasandani, P.; Mao, Z.H.; Jia, W.; Sun, M. Relationship between Triboelectric Charge and Contact Force for Two Triboelectric Layers. *J. Electrostat.* **2017**, *90*, 147–152. [CrossRef]
24. Hu, G.; Zhao, C.; Yang, Y.; Li, X.; Liang, J. Triboelectric Energy Harvesting Using an Origami-Inspired Structure. *Appl. Energy* **2022**, *306*, 118037. [CrossRef]
25. Pongampai, S.; Pakawanit, P.; Charoonsuk, T.; Hajra, S.; Kim, H.J.; Vittayakorn, N. Design and Optimization of Miura-Origami-Inspired Structure for High-Performance Self-Charging Hybrid Nanogenerator. *J. Sci. Adv. Mater. Devices* **2023**, *8*, 100618. [CrossRef]
26. Xie, L.; Zhai, N.; Liu, Y.; Wen, Z.; Sun, X. Hybrid Triboelectric Nanogenerators: From Energy Complementation to Integration. *Research* **2021**, *2021*, 9143762. [CrossRef]